PNAS RESEARCH ARTICLE | MEDICAL SCIENCES

The lipoprotein lipase that is shuttled into capillaries by GPIHBP1 enters the glycocalyx where it mediates lipoprotein processing

Wenxin Song[a], Anne P. Beigneux[a], Thomas A. Weston[a], Kai Chen[b,c], Ye Yang[a], Le Phuong Nguyen[a], Paul Guagliardo[d], Hyesoo Jung[a], Anh P. Tran[a], Yiping Tu[a], Caitlyn Tran[a], Gabriel Birrane[e], Kazuya Miyashita[f], Katsuyuki Nakajima[f], Masami Murakami[f], Peter Tontonoz[g], Haibo Jiang[b], Michael Ploug[h,i], Loren G. Fong[a,1], and Stephen G. Young[a,j,1]

Contributed by Stephen G. Young; received August 20, 2023; accepted September 19, 2023; reviewed by Jay D. Horton and Rudolf Zechner

Lipoprotein lipase (LPL), the enzyme that carries out the lipolytic processing of triglyceride-rich lipoproteins (TRLs), is synthesized by adipocytes and myocytes and secreted into the interstitial spaces. The LPL is then bound by GPIHBP1, a GPI-anchored protein of endothelial cells (ECs), and transported across ECs to the capillary lumen. The assumption has been that the LPL that is moved into capillaries remains attached to GPIHBP1 and that GPIHBP1 serves as a platform for TRL processing. In the current studies, we examined the validity of that assumption. We found that an LPL-specific monoclonal antibody (mAb), 88B8, which lacks the ability to detect GPIHBP1-bound LPL, binds avidly to LPL within capillaries. We further demonstrated, by confocal microscopy, immunogold electron microscopy, and nanoscale secondary ion mass spectrometry analyses, that the LPL detected by mAb 88B8 is located within the EC glycocalyx, distant from the GPIHBP1 on the EC plasma membrane. The LPL within the glycocalyx mediates the margination of TRLs along capillaries and is active in TRL processing, resulting in the delivery of lipoprotein-derived lipids to immediately adjacent parenchymal cells. Thus, the LPL that GPIHBP1 transports into capillaries can detach and move into the EC glycocalyx, where it functions in the intravascular processing of TRLs.

triglycerides | GPIHBP1 | lipoprotein lipase | endothelial cells

Lipoprotein lipase (LPL), the enzyme that carries out the lipolytic processing of triglyceride-rich lipoproteins (TRLs), is synthesized primarily by myocytes and adipocytes and secreted into the interstitial spaces. GPIHBP1, a GPI-anchored protein of capillary endothelial cells (ECs), captures the interstitial LPL and shuttles it across ECs to its site of action within the capillary lumen (1, 2). The binding of LPL by GPIHBP1 is understood in detail, thanks to a crystal structure of the LPL–GPIHBP1 complex (3) and biophysical analyses of LPL–GPIHBP1 interactions (4–7). GPIHBP1's three-fingered LU (Ly6/uPAR) domain binds in a specific fashion, largely by hydrophobic contacts, to LPL's carboxyl-terminal lipid-binding domain (8–10). GPIHBP1's N-terminal acidic domain, which contains a sulfated tyrosine and many aspartates and glutamates, contributes to LPL binding (4, 11). The acidic domain binds, by electrostatic forces, to a large basic patch on the surface of LPL (3) and increases the affinity of LPL–GPIHBP1 interactions (4, 11). GPIHBP1's acidic domain also stabilizes the conformation of LPL's catalytic domain and preserves catalytic activity (4, 11). Finally, the acidic domain is important for LPL transport across ECs (12). In the absence of the acidic domain, LPL's large basic patch is left exposed and free to bind to negatively charged heparan sulfate proteoglycans (HSPGs) on the abluminal surface of capillaries, limiting LPL movement across ECs (12). GPIHBP1's acidic domain sheathes LPL's basic patch, thereby abrogating abluminal HSPG interactions and freeing GPIHBP1•LPL complexes to move to the capillary lumen (12).

Following the identification of GPIHBP1 as an LPL-binding protein (1), the prevailing assumption has been that LPL remains attached to GPIHBP1 and that GPIHBP1 functions as a "platform" for the processing of TRLs (1). This assumption seemed reasonable. First, early confocal micrographs of mouse tissues revealed strong colocalization of LPL and GPIHBP1 along the luminal surface of capillary ECs (2). Second, GPIHBP1-bound LPL is catalytically active (4, 13, 14), and the binding of LPL to GPIHBP1 stabilizes LPL activity (4, 5). Third, the notion that LPL remains attached to GPIHBP1 was consistent with the fact that LPL can be released into the bloodstream with a bolus of heparin (a sulfated glycosaminoglycan) (15). Heparin disrupts the electrostatic interactions that augment the affinity of LPL–GPIHBP1 interactions (4). Despite these considerations, we have harbored doubts about the primacy of GPIHBP1-bound LPL for TRL processing. We were not confident that the EC glycocalyx [a gelatinous heparan sulfate proteoglycan (HSPG)–rich structure that extends >250 nm into the capillary lumen (16)] would permit

Significance

Lipoprotein lipase (LPL) carries out the intravascular lipolytic processing of triglyceride-rich lipoproteins (TRLs), a physiologic process that delivers lipid nutrients to tissues. LPL is synthesized and secreted by parenchymal cells but is subsequently captured by an endothelial cell (EC) protein, GPIHBP1, and moved to the capillary lumen. LPL is generally assumed to remain attached to GPIHBP1, but the precise location of LPL in capillaries has never been studied. Using confocal microscopy, immunogold EM, and NanoSIMS (nanoscale secondary ion mass spectrometry) analyses, we found that much of the LPL that GPIHBP1 shuttles into capillaries detaches and is captured within the EC glycocalyx. "Glycocalyx LPL" mediates TRL margination and processing and results in the delivery of TRL-derived lipid nutrients to parenchymal cells.

Author contributions: W.S., P.T., H.J., M.P., L.G.F., and S.G.Y. designed research; W.S., A.P.B., T.A.W., K.C., Y.Y., L.P.N., P.G., H.J., A.P.T., Y.T., C.T., H.J., M.P., and S.G.Y. performed research; W.S., A.P.B., Y.Y., G.B., K.M., K.N., M.M., M.P., and S.G.Y. contributed new reagents/analytic tools; W.S., A.P.B., P.T., H.J., M.P., L.G.F., and S.G.Y. analyzed data; and W.S., A.P.B., M.P., L.G.F., and S.G.Y. wrote the paper.

Reviewers: J.D.H., University of Texas Southwestern Medical Center; and R.Z., Karl-Franzens-Universitat Graz.

Competing interest statement: S.G.Y. is scientific advisory board member of Kyttaro, Inc. K.N. holds stock in Immuno-Biological Laboratories and serves as a consultant for Skylight and Sysmex.

[1]To whom correspondence may be addressed. Email: lfong@mednet.ucla.edu or sgyoung@mednet.ucla.edu.

This article contains supporting information online at https://www.pnas.org/lookup/suppl/doi:10.1073/pnas.2313825120/-/DCSupplemental.

Published October 23, 2023.

TRLs [some with diameters >500 nm (17)] to come into contact with GPIHBP1•LPL complexes on the luminal plasma membrane (PM) of ECs. Furthermore, we were not confident that the LPL within capillaries would remain attached to GPIHBP1. Surface plasmon resonance studies with purified proteins revealed that the GPIHBP1•LPL complex has a half-life of 1.9 min at 20 °C, such that ~one-half of the LPL dissociates from GPIHBP1 every 2 min (11). If LPL were to detach from GPIHBP1 in vivo, it seemed conceivable to us that the LPL could be captured by negatively charged HSPGs in the glycocalyx.

In the years following the identification of LPL as an intravascular heparin-releasable enzyme (4), LPL was presumed to be bound, by electrostatic interactions, to the luminal surface of blood vessels, but the location of LPL in blood vessels was unclear. Several immunohistochemistry studies concluded that LPL was located in virtually all blood vessels, including large arteries and blood vessels of the brain (18–21), but we now recognize that is not the case and that LPL is confined to capillaries of peripheral tissues (where GPIHBP1 is expressed) (1, 2). An immunogold EM study, published >15 y before GPIHBP1's role in lipolysis was uncovered (22), used chicken antibodies against bovine LPL (along with a rabbit secondary antibody and a gold-conjugated goat tertiary antibody) to visualize LPL in the mouse heart. Gold nanoparticles were detected in cardiomyocytes and in capillaries (where they appeared to be concentrated on EC "processes" that extended into the capillary lumen). Unfortunately, the images of capillaries were limited and the morphology was difficult to interpret. Also, chicken antibodies against bovine LPL were later shown to be contaminated by antibodies against antithrombin III (23), a heparin-binding plasma protein that is known to bind to HSPGs on the surface of ECs (24).

In the current study, we used monospecific LPL antibodies, super-resolution confocal microscopy, immunogold electron microscopy, and nanoscale secondary ion mass spectrometry (NanoSIMS) analyses to define the location of LPL within capillaries. We were interested in determining whether some of the LPL that is shuttled into capillaries by GPIHBP1 detaches and enters the glycocalyx and, if so, whether the glycocalyx-bound LPL is relevant to the margination of TRLs along capillaries and to the delivery of TRL-derived lipid nutrients to parenchymal cells.

Results

LPL and GPIHBP1 Expression in Capillaries. We examined the binding of two LPL-specific monoclonal antibodies (mAbs), 5D2 and 88B8, to hLPL in tissues of *Lpl*$^{-/-}$ mice harboring a hLPL transgene driven by the muscle creatine kinase promoter (*Lpl*$^{-/-}$MCK–hLPL) (25). In those mice, the hLPL is expressed at low levels in the heart (25). The hLPL that is produced by cardiomyocytes is captured by GPIHBP1 and shuttled into capillaries by GPIHBP1. The epitope for 5D2 is located in a C-terminal Trp-rich loop that is distant from LPL's GPIHBP1-binding domains (26); hence, 5D2 binds both free and GPIHBP1-bound LPL (*SI Appendix,* Fig. S1*A*). 88B8 binds to LPL's GPIHBP1-binding domain (7); consequently, it cannot detect GPIHBP1-bound LPL (*SI Appendix,* Fig. S1*A*). 88B8 abolishes LPL binding to GPIHBP1 in cell-based (*SI Appendix,* Fig. S1*B*) and cell-free assays (*SI Appendix,* Fig. S1*C*).

We gave *Lpl*$^{-/-}$MCK–hLPL mice an intravenous injection of 88B8, 5D2, and the GPIHBP1-specific mAb 11A12 (each labeled with an Alexa Fluor dye). [11A12 binds to the C-terminus of GPIHBP1, distant from sequences involved in LPL binding (8)]. After 2 min, the vasculature was perfused with PBS, and tissue sections were prepared for fluorescence microscopy. 88B8, 5D2, and 11A12 bound to capillaries of the heart and skeletal muscle (Fig. 1*A*), but there was no binding to larger blood vessels (detected by the CD31-specific mAb 2H8) (Fig. 1*B*) or to capillaries of the brain (*SI Appendix*, Fig. S2). Of note, the hLPL inside heart capillaries of *Lpl*$^{-/-}$MCK–hLPL mice had been transported into capillaries by GPIHBP1, evident by the fact that there was no 88B8 or 5D2 binding to the capillary lumen in *Gpihbp1*$^{-/-}$*Lpl*$^{+/-}$MCK–hLPL mice (*SI Appendix*, Fig. S3) and by the fact that hLPL and mouse LPL (mLPL) in those mice were trapped within the interstitial spaces surrounding cardiomyocytes (*SI Appendix*, Fig. S4). [LPL distribution was examined in *Gpihbp1*$^{-/-}$*Lpl*$^{+/-}$MCK–hLPL

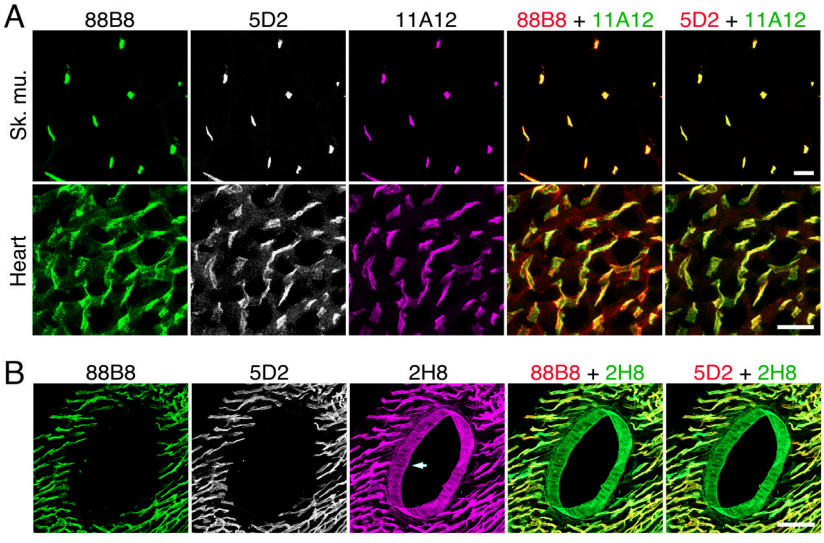

Fig. 1. Confocal micrographs of mAb 88B8 and 5D2 binding to capillaries of *Lpl*$^{-/-}$MCK–hLPL mice. (*A*) Fluorescent micrographs showing binding of mAbs 88B8, 5D2, and 11A12 to the luminal surface of blood vessels. Alexa Fluor 647–88B8 (*green*), Alexa Fluor 555–5D2 (*white*), and Alexa Fluor 488–11A12 (*magenta*) were injected intravenously into *Gpihbp1*$^{+/+}$*Lpl*$^{-/-}$MCK–hLPL mice. After 2 min, the mice were perfused with PBS and perfusion-fixed with PFA. mAbs 88B8, 5D2, and 11A12 bound to skeletal muscle and heart capillaries of *Gpihbp1*$^{+/+}$*Lpl*$^{-/-}$MCK–hLPL mice. Sk. mu., skeletal muscle. (Scale bar, 20 μm.) (*B*) Fluorescent micrographs showing binding of mAbs 88B8 and 5D2 to heart capillaries in *Gpihbp1*$^{+/+}$*Lpl*$^{-/-}$MCK–hLPL mice but not to CD31-positive larger blood vessels (detected by 2H8, *arrow*). (Scale bar, 50 μm.)

mice because *Gpihbp1*$^{-/-}$*Lpl*$^{-/-}$MCK–hLPL mice, like *Lpl*$^{-/-}$ mice (27), do not survive after birth.]

The rapid binding (within 2 min) of 88B8 to the capillary lumen cannot be explained by proposing that 88B8 detaches LPL from GPIHBP1, thereby permitting LPL to move onto other binding sites. First, 88B8 does not bind to GPIHBP1 in GPIHBP1-transfected cells (*SI Appendix*, Fig. S1 *A* and *B*). Second, 88B8 binds to LPL along the luminal surface of capillaries in *Lpl*$^{-/-}$ MCK–hLPL mice *after* perfusion-fixation of the vasculature with PFA (*SI Appendix*, Fig. S5).

The Binding of mAbs 88B8 and 5D2 to Capillaries Is Distinct. The fact that 88B8 binds to hLPL along capillaries in *Lpl*$^{-/-}$ MCK–hLPL mice implied the existence of a pool of hLPL that was not attached to GPIHBP1. To understand the binding of 88B8 to capillaries, we imaged heart capillary cross-sections with super-resolution microscopy. The binding of 88B8 to capillaries exhibited a "lumpy–bumpy" pattern and extended into the capillary lumen, away from 11A12 binding to GPIHBP1 on the luminal PM of ECs (Fig. 2*A* and *SI Appendix*, Fig. S6). In the images shown in Fig. 2*A* and *SI Appendix*, Fig. S6, there was minimal overlap between 88B8 and 11A12 binding, and Pearson correlation coefficients were low (Fig. 2*B*). 5D2 bound to the hLPL detected by 88B8, but colocalization with 11A12 was also observed, reflecting 5D2's capacity to bind GPIHBP1-bound LPL. An analysis of 16 capillary cross-sections revealed that 30.4 ± 2.0% of the LPL in capillaries that was detected by 5D2 was also detected by 88B8 (mean ± SEM), implying that ~30% of the intracapillary LPL is not attached to GPIHBP1.

We performed similar studies in *Lpl*$^{-/-}$ Tie2–hLPL mice, which express hLPL in ECs (30). Those mice were given an intravenous injection of Alexa Fluor–labeled 88B8, 5D2, and 11A12; then, after 2 min, the vasculature was perfused, cryosections were prepared, and mAb binding was assessed by fluorescence microscopy (*SI Appendix*, Fig. S7). 88B8 bound to "patches" of LPL that extended into the capillary lumen, away from 11A12 binding to GPIHBP1 on the luminal PM (*SI Appendix*, Fig. S8*A*). 5D2 bound to the same patches detected by 88B8, but in addition, there was colocalization of 5D2 with 11A12, reflecting 5D2's ability to bind GPIHBP1-bound LPL (*SI Appendix*, Fig. S8*A*). We performed the same studies in *Gpihbp1*$^{-/-}$*Lpl*$^{-/-}$Tie2–hLPL mice, except that the mice were infused with mAb 2H8 rather than 11A12. In those mice, the 88B8 and 5D2 binding patterns were identical, with the binding of both antibodies extending into the capillary lumen, away from 2H8 binding to CD31 on the luminal PM (*SI Appendix*, Fig. S8*B*).

In the hLPL transgenic mouse models, we suspected that 88B8 was binding to hLPL in the EC glycocalyx. To explore that idea, we performed immunogold EM studies. We injected 10-nm gold nanoparticle–88B8 into isolated hearts of *Lpl*$^{-/-}$MCK–hLPL

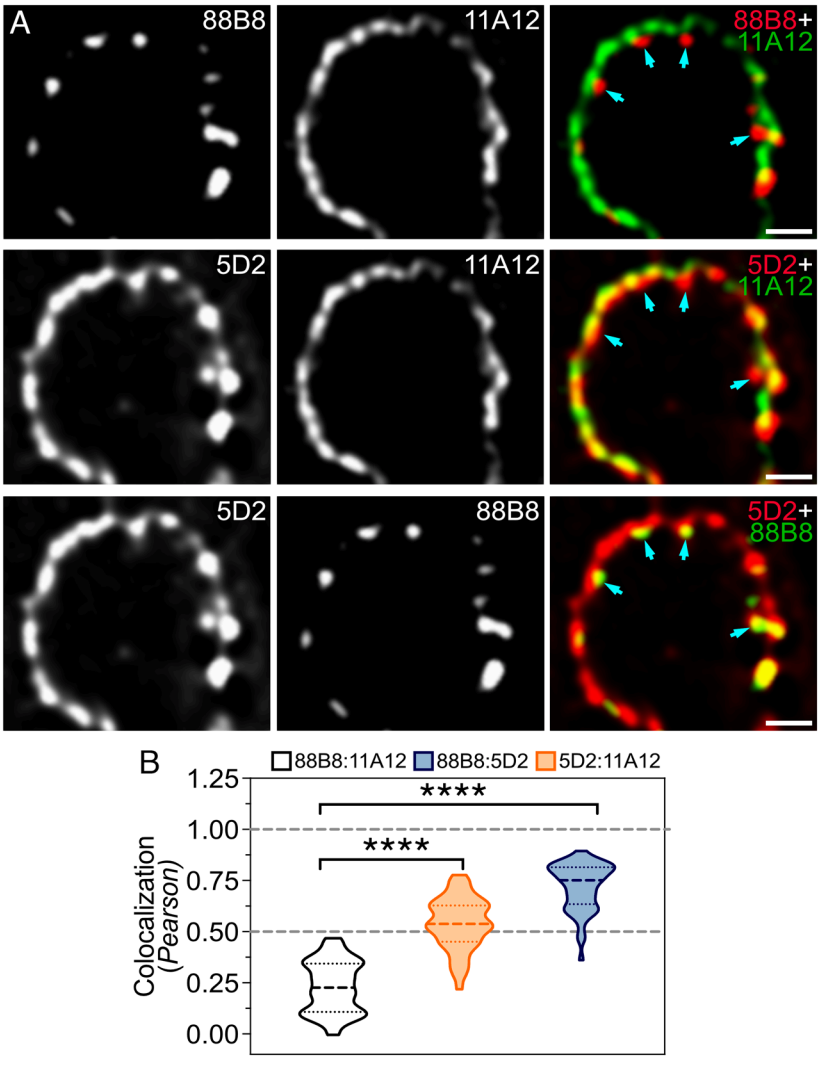

Fig. 2. mAb 88B8 binding to heart capillaries in *Lpl*$^{-/-}$MCK–hLPL mice projects toward the capillary lumen, away from mAb 11A12 binding to GPIHBP1 on the luminal PM. (*A*) Confocal micrographs of a capillary cross-section from an *Lpl*$^{-/-}$MCK–hLPL mouse after an intravenous injection of two hLPL-specific mAbs (Alexa Fluor 647–88B8, Alexa Fluor 555–5D2) and a GPIHBP1-specific mAb (Alexa Fluor 488–11A12). The binding of 88B8 to the capillary lumen exhibited a lumpy-bumpy pattern (*arrows*), extending toward the capillary lumen and away from 11A12 binding to GPIHBP1 on the luminal PM of the EC. 5D2 bound to the same pool of hLPL detected by 88B8 but in addition bound to GPIHBP1-bound LPL on the luminal PM. (Scale bar, 1 μm.) (*B*) Violin plot showing Pearson correlation coefficients for 88B8:11A12, 5D2:11A12, and 88B8:5D2 binding, where 1.0 is complete colocalization and 0.0 is absent colocalization. The minimal Pearson coefficient value for significant colocalization is 0.5 (horizontal dashed line) (28, 29). Correlation coefficients were calculated from 54 capillary cross-sections. The violin plot shows the median and interquartile range. ****$P < 0.0001$ by one-way ANOVA.

and wild-type mice, followed by perfusion of the vasculature, staining of the glycocalyx with $LaCl_3/DyCl_3$, and glutaraldehyde fixation. By transmission EM, numerous 88B8–gold nanoparticles were detected in the glycocalyx of heart capillary ECs in *Lpl*$^{-/-}$MCK–hLPL mice but not wild-type mice (Fig. 3 and *SI Appendix*, Fig. S9). There was no binding of an irrelevant gold-conjugated rat mAb [3C8, against mouse prelamin A (31)] to the glycocalyx (*SI Appendix*, Fig. S10). When gold nanoparticle–11A12 was injected into isolated hearts, nearly all of the gold was located within 20 nm of the luminal PM [the size of an IgG is ~14 nm (32)] (*SI Appendix*, Fig. S11). When gold nanoparticle–5D2 was injected into hearts of *Lpl*$^{-/-}$MCK–hLPL mice, gold nanoparticles were observed in the glycocalyx and adjacent to the EC PM (Fig. 3).

We also used backscattered electron (BSE) imaging with a scanning electron microscope to examine binding of 10-nm gold nanoparticle–88B8 to heart capillaries of *Lpl*$^{-/-}$MCK–hLPL mice. Again, many gold nanoparticles were located in the glycocalyx (*SI Appendix*, Fig. S12). Following BSE imaging, the elemental composition of the sections was examined by NanoSIMS, which makes it possible to create high-resolution images (33) based solely on the isotopic content of the tissue. Consistent with the BSE images, ^{197}Au–88B8 was detected in the glycocalyx (Fig. 4 and *SI Appendix*, Fig. S13*A*). The $^{133}Cs^+$ beam of the NanoSIMS instrument dislodges $^{197}Au^-$ ions (from gold nanoparticle–88B8) efficiently but $^{164}Dy^{16}O^-$ and $^{139}La^{16}O^-$ ions (from the $LaCl_3/DyCl_3$-stained glycocalyx) inefficiently, but we were still able to create images from $^{197}Au^-$ ions and from the sum of $^{164}Dy^{16}O^-$ and $^{139}La^{16}O^-$ ions. The $^{197}Au^-$ ions overlapped with the $^{164}Dy^{16}O^- + {}^{139}La^{16}O^-$ ions within the glycocalyx

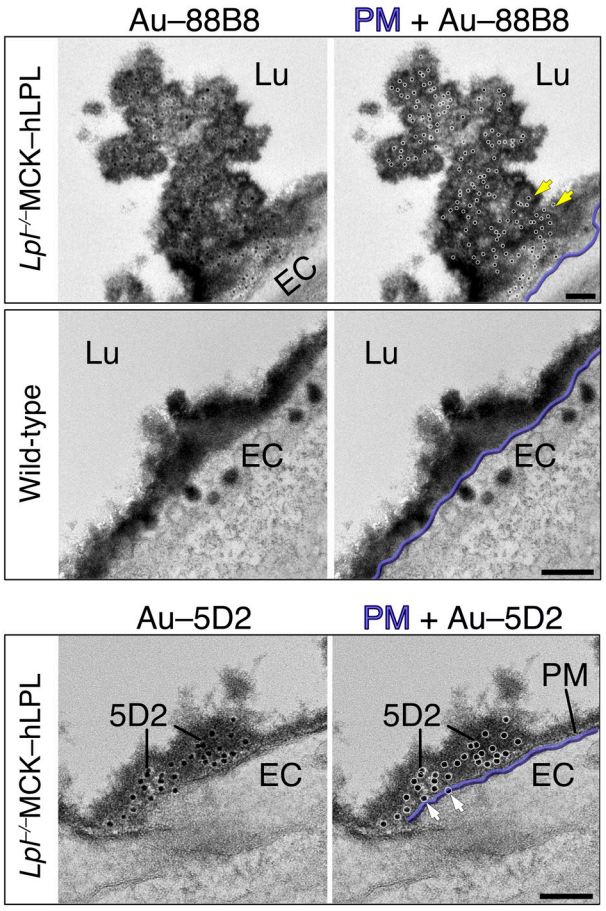

Fig. 3. Immunogold electron micrographs showing binding of gold-conjugated 88B8 and 5D2 to the glycocalyx of heart capillaries in *Lpl*$^{-/-}$MCK–hLPL mice. *Lpl*$^{-/-}$MCK–hLPL and wild-type mice were injected with 10-nm gold nanobead–conjugated 88B8 or 5D2. The glycocalyx (Gx) was stained with $LaCl_3/DyCl_3$. For clarity, each micrograph is shown in duplicate; on the right, nanoparticles are outlined by a *white* circle, and the EC PM is colored *purple*. In heart capillaries of *Lpl*$^{-/-}$MCK–hLPL mice (but not wild-type mice), gold-conjugated 88B8 bound to LPL in the glycocalyx (*yellow* arrows). Gold-conjugated 5D2 bound to LPL in the glycocalyx and to LPL on the luminal PM (*white* arrows), reflecting 5D2's ability to detect GPIHBP1-bound LPL. (Scale bar, 100 nm.)

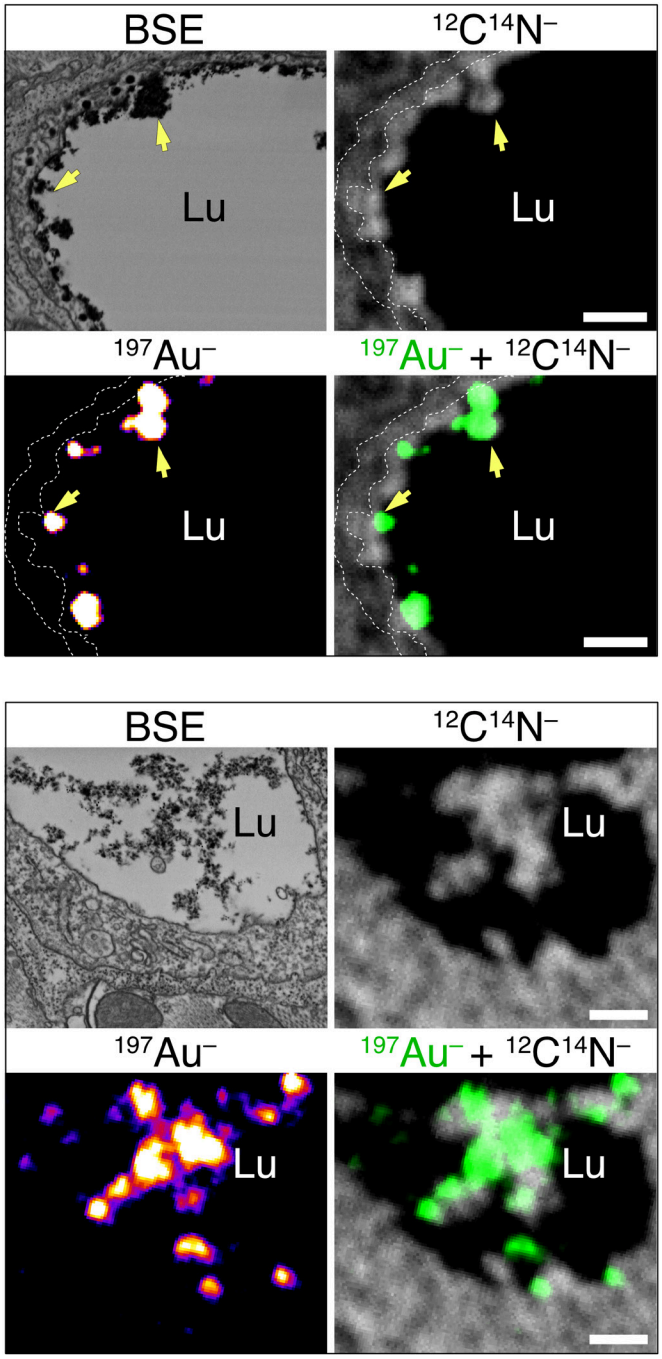

Fig. 4. BSE and NanoSIMS imaging showing binding of 10-nm gold nanoparticle–88B8 to LPL on the luminal surface of heart capillaries in *Lpl*$^{-/-}$MCK–hLPL mice. Shown here are correlative BSE and NanoSIMS images of two different heart capillaries in *Lpl*$^{-/-}$MCK–hLPL mice that had been injected with 10-nm gold nanoparticle–88B8, followed by perfusion with PBS, fixation, and $LaCl_3/DyCl_3$ staining of the glycocalyx. The $^{12}C^{14}N^-$ NanoSIMS images were useful for morphology. In the capillary cross-section on the top, ^{197}Au was detected in the EC glycocalyx [*yellow* arrows in the capillary lumen (LU)]. The EC glycocalyx was detected in the BSE image and in the $^{12}C^{14}N^-$ NanoSIMS image. The white dashed line outlines the capillary EC. In the capillary cross-section on the bottom, ^{197}Au was detected in the EC glycocalyx, reflecting 88B8 binding to LPL in the glycocalyx. (Scale bars, 500 nm.)

(*SI Appendix*, Fig. S13 *A* and *B*). When gold nanoparticles were detected in the glycocalyx in BSE images, ^{197}Au was detected by NanoSIMS (Fig. 4 and *SI Appendix*, Fig. S13 *A–C*).

mLPL Is Also Located in the Glycocalyx. A rat mAb against mLPL (27A7) and a rabbit polyclonal antibody against mLPL (Ab3174) were used to define the intravascular location of mLPL. Both antibodies bind native mLPL, evident from their ability to immunoprecipitate freshly secreted LPL and GPIHBP1•LPL complexes (*SI Appendix*, Fig. S14*A*). 27A7 binds to GPIHBP1-bound mLPL in cell-free (*SI Appendix*, Fig. S14*B*) and cell-based assays (*SI Appendix*, Fig. S14*C*). Antibodies 27A7 and Ab3174 are specific for mLPL and do not detect hLPL (*SI Appendix*, Fig. S14*D*). SPR studies revealed that 27A7 binds mLPL•mGPIHBP1 complexes with subnanomolar affinity but does not bind hLPL•hGPIHBP1 complexes (*SI Appendix*, Fig. S15*A*). SPR studies also revealed that 27A7 binds to the Trp-rich loop in the C-terminus of mLPL; the binding of 27A7 to mLPL (but not hLPL) appears to depend on the presence of a proline in the Trp-rich loop (*SI Appendix*, Fig. S15 *B* and *C*).

To determine whether mLPL is located in the glycocalyx, we gave $Lpl^{+/-}$MCK–hLPL mice an intravenous injection of Alexa Fluor–labeled 88B8, 27A7, and 11A12. As expected, 88B8 bound to hLPL in the glycocalyx—away from 11A12 on the surface of ECs (*SI Appendix*, Fig. S16*A*). 27A7 also bound to mLPL in the glycocalyx (colocalizing with 88B8), but in addition, there was colocalization with 11A12 (*SI Appendix*, Fig. S16*A*), consistent with 27A7's ability to bind GPIHBP1-bound mLPL. Pearson correlation coefficients, generated from 70 capillary cross sections, revealed negligible 88B8–11A12 colocalization but substantial 27A7–11A12 and 88B8–27A7 colocalization (*SI Appendix*, Fig. S16*B*). An analysis of capillary cross-sections (n = 8) revealed that 27.2 ± 3.8% of the LPL in capillaries that was detected by 27A7 was also detected by 88B8 (mean ± SEM), implying that 25 to 30% of the intracapillary mLPL is not attached to GPIHBP1.

We gave wild-type mice an intravenous injection of 10-nm gold nanoparticle–27A7, followed by vascular perfusion and $LaCl_3$/$DyCl_3$ staining of the glycocalyx. Numerous 27A7–gold nanoparticles were present in the glycocalyx of heart capillaries (Fig. 5*A* and *SI Appendix*, Fig. S16*C*). We also performed correlative BSE/NanoSIMS imaging of heart capillaries after infusing an isolated heart from a wild-type mouse with 1.4-nm gold–Ab3174 and [^{15}N]11A12, followed by PBS perfusion and $LaNO_3$/$DyCl_3$ staining. BSE imaging revealed strong staining of the glycocalyx, and NanoSIMS analyses revealed a strong $^{12}C^{14}N^-$ signal in the EC glycocalyx (reflecting $LaNO_3$ staining) (Fig. 5*B* and *SI Appendix*, Fig. S17*A*). ^{197}Au was detected in the glycocalyx but was also present at the luminal surface of capillaries (reflecting Ab3174 binding to GPIHBP1-bound LPL) (Fig. 5*B* and *SI Appendix*, Fig. S17 *A–C*). In this experiment, we observed enrichment of $^{12}C^{15}N^-$ ions at the boundary between the EC and the glycocalyx (*SI Appendix*, Fig. S17*C*), reflecting [^{15}N]11A12 binding to GPIHBP1 on the surface of ECs. The distributions of ^{15}N enrichment and ^{197}Au in capillaries were distinct; the overlap between ^{197}Au-labeled 3174 and the glycocalyx was greater than the overlap between [^{15}N]11A12 and the glycocalyx (*SI Appendix*, Fig. S17*D*).

GPIHBP1 is required for transporting LPL into capillaries (Fig. 1*A* and *SI Appendix*, Fig. S3), but our studies indicated that some of that LPL detaches and enters the HSPG-rich glycocalyx. To explore the plausibility of LPL release from GPIHBP1 and its subsequent capture by sulfated glycosaminoglycans, we performed in vitro studies. We coupled mAb 11A12 to agarose beads; loaded the 11A12-coated beads with GPIHBP1•LPL complexes; washed the beads; and then incubated the 11A12–GPIHBP1•LPL beads with heparin-coated magnetic beads. After 30 min, we observed transfer of LPL onto the heparin-coated beads (see lane 3, *SI Appendix*, Fig. S18).

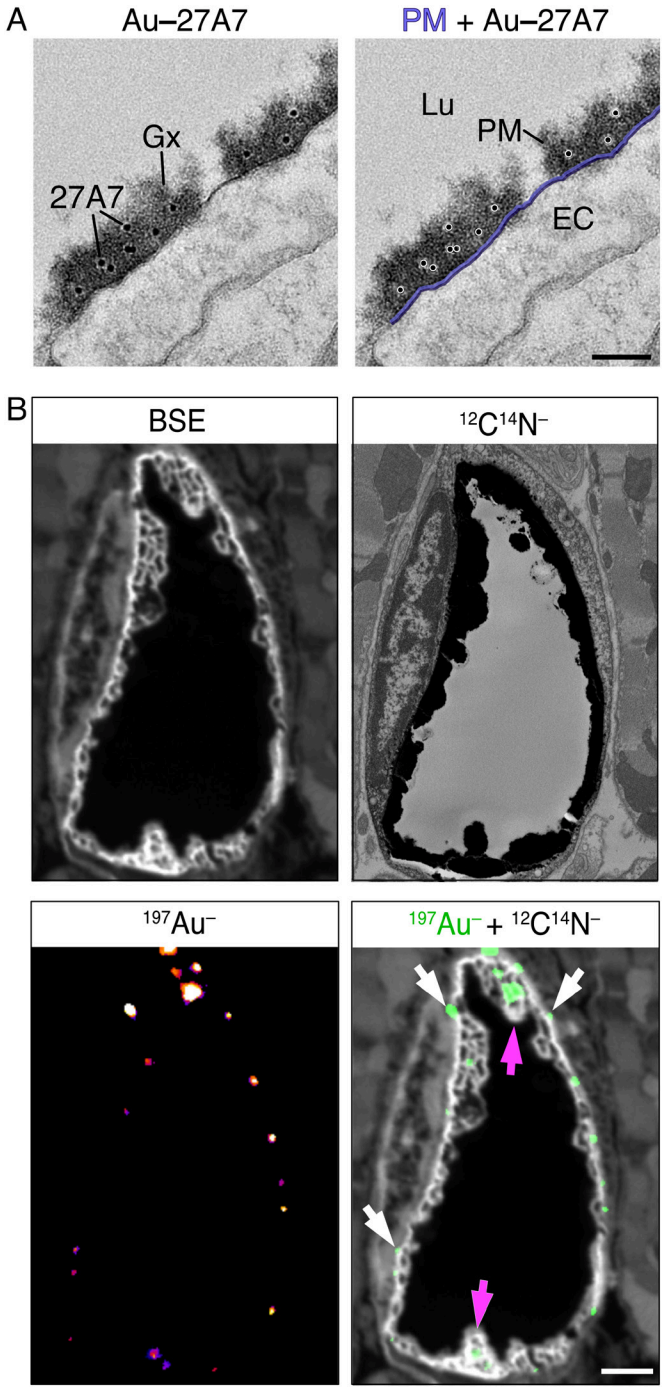

Fig. 5. mLPL is located within the glycocalyx. (*A*) Electron micrographs of heart capillaries of a wild-type mouse after an intravenous injection of 10-nm gold nanoparticle–27A7, revealing nanoparticles in the $LaCl_3$/$DyCl_3$-stained glycocalyx (Gx). In the duplicate images, the gold nanoparticles were highlighted with *white* circles and the PM was colored *purple*. (Scale bar, 100 nm.) Lu, lumen; EC, endothelial cell. (*B*) Correlative BSE and NanoSIMS imaging of a capillary after perfusing an isolated heart from a wild-type mouse with 1.4-nm gold–conjugated Ab3174 (followed by glycocalyx staining with $LaNO_3$/$DyCl_3$). Binding of Ab3174 to intravascular LPL was detected with a $^{197}Au^-$ NanoSIMS image. Ab3174 was located both on the EC PM (*white* arrows) and in the glycocalyx (*magenta* arrows). The glycocalyx was delineated in the BSE image and in the $^{12}C^{14}N^-$ NanoSIMS image (reflecting strong $LaNO_3$ staining). (Scale bars, 1 μm.)

The Glycocalyx Pool of LPL Remains in the Capillary Lumen and Does Not Move "Backward" to the Abluminal Surface of Capillaries. In earlier studies (2, 34), we found that 11A12, when injected into a BAT pad of a living mouse, moves in a GPIHBP1-dependent fashion to the luminal surface of capillaries. When 11A12 is injected intravenously, it is captured by GPIHBP1 and moves to the abluminal surface of ECs. Whether *intracapillary* LPL moves (along with GPIHBP1) to the abluminal surface of capillary ECs is unknown. To explore the mobility of intracapillary LPL, *Lpl*$^{-/-}$MCK–hLPL mice were given an intravenous injection of Alexa Fluor–labeled 11A12, 88B8, and 5D2. After 2 h, cryosections of BAT were prepared for microscopy. We observed 11A12 on the abluminal surface of ECs, indicating that GPIHBP1 had moved from the luminal to the abluminal surface of ECs (*SI Appendix*, Fig. S19). In contrast, 88B8 remained within the capillary lumen and did not appear on the abluminal surface of ECs (*SI Appendix*, Fig. S19). Like 11A12, 5D2 moved to the abluminal surface of ECs (*SI Appendix*, Fig. S19). Thus, in contrast to the glycocalyx LPL pool (detected by 88B8), the LPL that is attached to GPIHBP1 moved to the abluminal surface of ECs.

Recombinant hLPL, When Injected Intravenously, Binds to the Glycocalyx. To confirm the ability of LPL to bind to the glycocalyx, we infused isolated hearts of *Gpihbp1*$^{-/-}$ mice with recombinant, catalytically active hLPL (or normal saline alone), followed by an infusion of Alexa Fluor–labeled 88B8, 2H8, and 11A12. After 10 min, the vasculature was perfused with PBS, and sections were prepared for microscopy. 2H8 bound avidly to CD31 on the luminal surface of capillaries and larger blood vessels, but 11A12 binding was absent. In hearts that had been infused with hLPL, we observed avid binding of 88B8 to hLPL in capillaries but not larger blood vessels (Fig. 6*A*). Super-resolution microscopy revealed that 88B8 was bound to hLPL in the glycocalyx, distant from 2H8 on the luminal surface of ECs (Fig. 6*B* and *SI Appendix*, Fig. S20 *A* and *B*).

In parallel, we injected recombinant hLPL into isolated hearts of wild-type mice, followed by injections of Alexa Fluor–labeled 88B8, 27A7, and 2H8. All three mAbs bound avidly to the luminal surface of capillaries (*SI Appendix*, Fig. S21*A*). Super-resolution microscopy revealed 88B8 binding to tufts of glycocalyx, distant from 2H8 binding (*SI Appendix*, Fig. S21*B*). Of note, 27A7 detected endogenous mLPL in the same glycocalyx tufts, but there was also colocalization of 27A7 with 2H8, consistent with 27A7's ability to bind GPIHBP1-bound mLPL (*SI Appendix*, Fig. S21*B*). Pearson correlation coefficients revealed substantial 27A7:CD31 and 88B8:27A7 colocalization but negligible 88B8:CD31 colocalization (*SI Appendix*, Fig. S21*C*). 27A7 binding was confined to capillaries (*SI Appendix*, Fig. S21*A*), consistent with the fact that GPIHBP1 (and LPL transport) are restricted to capillary ECs (2, 35). Of note, the binding of 88B8 to hLPL in the glycocalyx was also confined to capillaries, implying that the glycocalyx of larger blood vessels has little capacity to bind hLPL (*SI Appendix*, Fig. S21*A*).

Glycocalyx LPL Mediates TRL Margination. The margination of Alexa Fluor–labeled TRLs along capillaries is robust in wild-type mice but virtually absent in *Gpihbp1*$^{-/-}$ mice (35) [where intracapillary LPL is absent (2)]. We hypothesized that glycocalyx LPL could be important for TRL margination. If that were the case, we reasoned that TRLs would marginate along heart capillaries of *Gpihbp1*$^{-/-}$ mice after loading the glycocalyx with hLPL. To test that idea, we gave *Gpihbp1*$^{-/-}$ mice an intravenous injection of recombinant hLPL (or normal saline alone) with a lipase inhibitor, followed by an infusion of the lipase inhibitor and Alexa Fluor–labeled TRLs, 88B8, and 2H8. In *Gpihbp1*$^{-/-}$ mice that were injected with hLPL, 88B8 binding to 2H8-positive capillaries

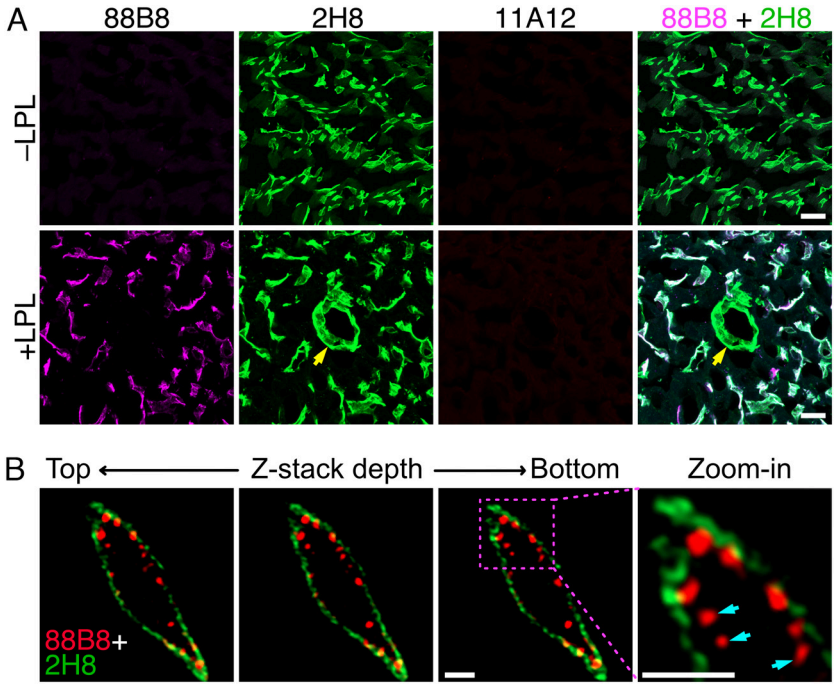

Fig. 6. Avid binding of recombinant hLPL to heart capillaries of a *Gpihbp1*$^{-/-}$ mouse. (*A*) Confocal micrographs of heart capillaries from an isolated heart of a *Gpihbp1*$^{-/-}$ mouse that had been injected intravenously with recombinant hLPL (+LPL) or normal saline alone (–LPL), followed by an infusion of Alexa Fluor 647–88B8, Alexa Fluor 488–2H8, and Alexa Fluor 555–11A12. hLPL (which was detected by 88B8) binds to capillaries of a *Gpihbp1*$^{-/-}$ mouse but not to larger blood vessels (*yellow arrow*). (Scale bar, 20 μm.) (*B*) Z-stack confocal micrographs of a capillary cross-section. Most of the 88B8 binding (*red*) was located in the capillary glycocalyx (arrows in the "zoom-in" image), extending toward the capillary lumen and away from 2H8 binding to CD31 (*green*) on the luminal PM of the EC. The boxed region is shown at a higher magnification on the *Right*. (Scale bars, 1 μm.)

was robust and was accompanied by TRL margination (Fig. 7*A*). 88B8 binding and TRL margination were absent in larger blood vessels (Fig. 7*A*). Super-resolution microscopy revealed 88B8 bound to LPL in the glycocalyx, away from 2H8 binding on the luminal PM of capillaries (Fig. 7*B* and *SI Appendix*, Fig. S22*A*). TRL margination colocalized with 88B8 binding (Fig. 7*B* and *SI Appendix*, Fig. S22*A*). Pearson correlation coefficients revealed negligible 88B8:CD31 and TRL:CD31 colocalization but strong 88B8:TRL colocalization (*SI Appendix*, Fig. S22*B*). Electron microscopy supported these findings. In wild-type mice, we observed margination of TRLs along the $LaCl_3/DyCl_3$-stained glycocalyx of heart capillaries (Fig. 7*C*). In *Gpihbp1*$^{-/-}$ mice that had been given an injection of hLPL (followed by an infusion of TRLs), electron micrographs of heart capillaries revealed margination of TRLs along the capillary EC glycocalyx (Fig. 7*C*). In many cases, the TRLs were trapped within the glycocalyx. No margination was observed in large blood vessels (*SI Appendix*, Fig. S23). In *Gpihbp1*$^{-/-}$ mice that had been given an injection of normal saline (followed by TRLs), TRL margination along capillaries was negligible or absent (Fig. 7*C*).

We created a mutant hLPL in which three tryptophans (W390A, W393A, and W394A) in LPL's carboxyl-terminal lipid-binding domain were replaced with alanine (3); these substitutions abolish LPL's ability to hydrolyze long-chain triglyceride substrates without affecting activity against soluble substrates (36). The tryptophan mutations are distant from LPL's basic patch (3). When the mutant hLPL was infused into *Gpihbp1*$^{-/-}$ mice, it bound avidly to the EC glycocalyx in BAT and heart capillaries but did not mediate TRL margination (*SI Appendix*, Fig. S24).

Capillary ECs of the brain do not express GPIHBP1 (2), and intracapillary LPL is absent in brain capillaries (*SI Appendix*, Fig. S25). We hypothesized that the glycocalyx of brain capillaries, like that of the glycocalyx of larger blood vessels in peripheral tissues, lacks the ability to bind recombinant hLPL (and therefore the ability to mediate TRL margination). To test this hypothesis, *Gpihbp1*$^{-/-}$ mice were given an intravenous injection of large amounts of wild-type hLPL followed by an infusion of Alexa Fluor–labeled 2H8, 88B8, and TRLs. We observed avid 88B8 binding to LPL in 2H8-positive capillaries of the heart, along with TRL margination along 88B8-positive capillaries (*SI Appendix*, Fig. S26). In contrast, there was no binding of 88B8 to 2H8-positive capillaries of the brain, nor was there TRL margination (*SI Appendix*, Fig. S26).

Glycocalyx LPL Can Mediate the Delivery of TRL-Derived Lipid Nutrients to Cardiomyocytes. While the infusion of recombinant hLPL into *Gpihbp1*$^{-/-}$ mice led to TRL margination in heart capillaries, the key issue was whether TRL processing by glycocalyx LPL results in the delivery of lipid nutrients to cardiomyocytes. To address this issue, we prepared [^{2}H]TRLs from the plasma of *Gpihbp1*$^{-/-}$ mice (after administering [^{2}H]mixed fatty acids for 4.5 d). The [^{2}H]TRLs were highly enriched in ^{2}H (>8,000-fold

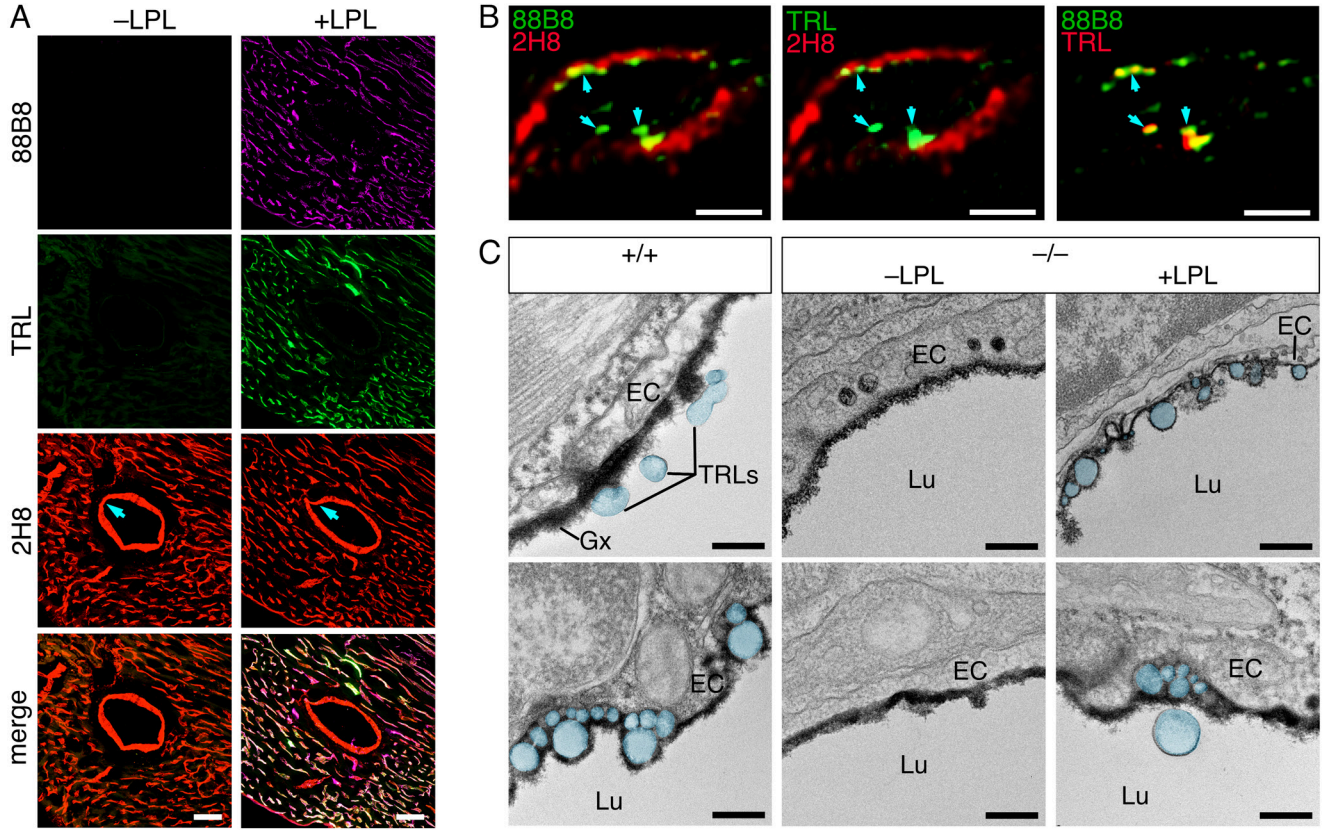

Fig. 7. TRL margination along heart capillaries. (*A*) Confocal micrographs of the heart of a *Gpihbp1*$^{-/-}$ mouse that had been injected intravenously with recombinant hLPL (+LPL) or normal saline alone (–LPL), followed by an infusion of Alexa Fluor 647–88B8 (*magenta*), Alexa Fluor 488–TRLs (*green*), and Alexa Fluor 555–2H8 (*red*). After 30 s, *Gpihbp1*$^{-/-}$ mice were euthanized; the vasculature was perfused with PBS; and the heart was harvested and prepared for microscopy. In the mice that were injected with normal saline, 88B8 binding was absent and TRL margination was negligible. In mice injected with recombinant hLPL, 88B8 binding and TRL binding in capillaries were robust. (Scale bar, 20 μm.) (*B*) Cross-section of a *Gpihbp1*$^{-/-}$ heart capillary from the experiment in *panel A*. 88B8 binding was located in tufts of glycocalyx, extending toward the capillary lumen and away from the binding of 2H8 to CD31 on the luminal PM. TRLs marginated along glycocalyx LPL (detected by 88B8). (Scale bar, 1 μm.) (*C*) Electron micrographs of heart capillaries from wild-type (+/+) and *Gpihbp1*$^{-/-}$ mice (–/–) that had been injected with recombinant hLPL (+LPL) or normal saline alone, followed by an infusion of TRLs. The glycocalyx (Gx) was stained with $LaCl_3/DyCl_3$. TRLs were colored *blue*. (Scale bar, 200 nm.) Lu, lumen; EC, endothelial cell.

greater than natural abundance). *Gpihbp1*$^{-/-}$ mice that had been maintained on a low-fat diet for 13 d (to reduce plasma triglyceride levels to ~500 mg/dL) were given an intravenous injection of hLPL (or normal saline alone). hLPL was undetectable in the plasma compartment after 3 min (*SI Appendix*, Fig. S27), consistent with our studies showing hLPL binds avidly to the glycocalyx lining of capillaries (Fig. 6 and *SI Appendix*, Fig. S21). At that time point, the mice were given an intravenous infusion of the [^{2}H]TRLs. After allowing the [^{2}H]TRLs to circulate for 3 min, the mice were euthanized, and resin-embedded sections were prepared for NanoSIMS analyses. In mice that had been injected with hLPL, NanoSIMS imaging revealed [^{2}H]TRL margination along capillaries and ^{2}H enrichment in mitochondria and cytosolic lipid droplets of cardiomyocytes (Fig. 8 and *SI Appendix*, Fig. S28*A*). ^{2}H enrichment in cardiomyocytes was significantly lower in mice that had been injected with normal saline rather than hLPL (Fig. 8 and *SI Appendix*, Fig. S28).

Discussion

In the years after LPL was characterized as a heparin-releasable triglyceride hydrolase (15, 37), the assumption was that LPL was bound, by electrostatic forces, to sulfated polysaccharides in blood vessels (38–40). This model was widely accepted, but it was incomplete. The model did not explain how LPL, which is secreted by myocytes and adipocytes, traversed ECs to reach the capillary lumen. Also, the location of LPL in blood vessels was unknown. Over the past 15 years, a series of discoveries has changed the model for plasma triglyceride metabolism. We found that *i*) a protein of capillary ECs, GPIHBP1, captures LPL and transports it to the capillary lumen (2); *ii*) GPIHBP1 binds LPL with great specificity, largely by hydrophobic contacts between GPIHBP1's LU domain and LPL's C-terminal lipid-binding domain (3, 8, 10, 41); *iii*) electrostatic interactions between GPIHBP1's acidic domain and LPL's large basic patch increase the affinity of these interactions (3, 4, 11, 42); *iv*) missense mutations that disrupt LPL–GPIHBP1 interactions prevent LPL transport and cause hypertriglyceridemia (3, 43–46); *v*) GPIHBP1 stabilizes LPL conformation and catalytic activity (3–5, 11); and *vi*) GPIHBP1-bound LPL is catalytically active (4, 13, 14). In light of these observations, it seemed likely that GPIHBP1 functioned as the binding site for LPL in capillaries and that it represented the platform for TRL processing. Our current studies show that it is not that simple. We found that much of the LPL that is transported into capillaries by GPIHBP1 enters the glycocalyx. The presence of LPL within the EC glycocalyx was documented by super-resolution microscopy, immunogold EM, and NanoSIMS analyses. We further demonstrated, by confocal and electron microscopy, that loading of the capillary glycocalyx of *Gpihbp1*$^{-/-}$ mice with catalytically active hLPL results in TRL margination in capillaries, and we showed, by NanoSIMS analyses, that [^{2}H]TRL processing along the hLPL-loaded glycocalyx of *Gpihbp1*$^{-/-}$ mice results in the delivery of [^{2}H]TRL-derived nutrients to adjacent cardiomyocytes. These findings have changed our understanding of intravascular lipolysis.

The observation that LPL moves from GPIHBP1 on the luminal surface of capillary ECs to the glycocalyx is consistent with biophysical studies. SPR experiments revealed that LPL's dissociation rate from GPIHBP1 is relatively high, such that half of the LPL detaches from GPIHBP1 every 2 min ($t_{1/2}$ of 1.9 min) (11). We also know that high concentrations of sulfated glycosaminoglycans are effective in capturing LPL from GPIHBP1 (36). When GPIHBP1•LPL complexes are loaded onto a heparin–Sepharose column, LPL

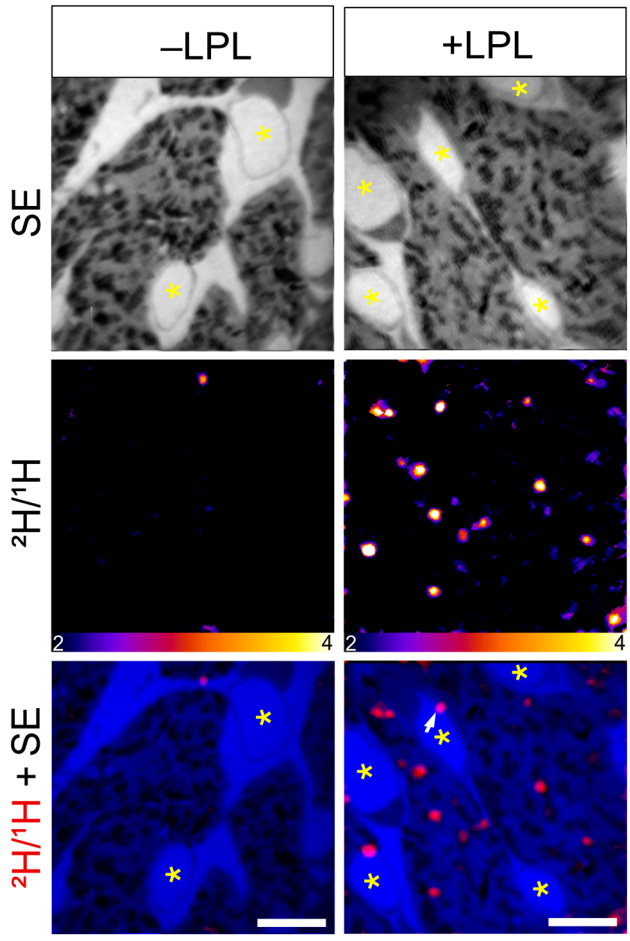

Fig. 8. NanoSIMS images showing delivery [^{2}H]TRL-derived lipids to cardiomyocytes in *Gpihbp1*$^{-/-}$ mice after an intravenous injection of recombinant wild-type hLPL. NanoSIMS images of heart capillaries from *Gpihbp1*$^{-/-}$ mice that had been injected intravenously with recombinant wild-type hLPL (+LPL) or normal saline (–LPL), followed by an infusion of [^{2}H]TRLs. Secondary electron (SE) images were useful for tissue morphology; capillaries are denoted by *yellow* asterisks. ^{2}H/^{1}H ratio images revealed [^{2}H]TRL margination along capillaries and entry of [^{2}H]TRL-derived lipids into surrounding cardiomyocytes. The scale shows the ^{2}H/^{1}H ratio multiplied by 10,000. Composite SE (*blue*) and ^{2}H/^{1}H (*red*) NanoSIMS images show margination of [^{2}H]TRLs in capillaries (*white* arrows) and the entry of ^{2}H-enriched lipids into cardiomyocytes.

detaches from GPIHBP1 and is captured by the heparin-coated beads (with free GPIHBP1 appearing in the "flow-through") (36). We suspect that this same phenomenon, LPL detachment from GPIHBP1 followed by binding to sulfated proteoglycans, occurs in capillaries and accounts for glycocalyx-bound LPL.

LPL is required for TRL margination along capillaries, evident from the virtual absence of TRL margination in capillaries of *Gpihbp1*$^{-/-}$ mice (where intravascular LPL is absent) (35, 47). In the current studies, we showed that LPL in the glycocalyx can mediate TRL margination, obviating a requirement for TRLs to traverse the glycocalyx and reach the luminal PM of ECs. We observed robust TRL margination along the glycocalyx of heart capillary ECs in wild-type mice and *Gpihbp1*$^{-/-}$ mice after loading of the glycocalyx with hLPL. Many of our electron micrographs suggested that TRLs had become embedded in the glycocalyx, which could allow TRL particles to be "attacked" by LPL from every direction. This proposition would align with biochemical studies suggesting that >40 LPL molecules are required for rapid TRL processing (48).

Our studies revealed that LPL's carboxyl-terminal Trp-rich lipid-binding loop [known to be required for triglyceride

hydrolysis (3, 35, 49, 50)] is crucial for TRL margination. We produced a mutant hLPL in which three tryptophans (W390, W393, and W394) were replaced with alanine (36). These mutations abolish the ability of LPL to hydrolyze triglycerides (36). When the mutant LPL was infused into *Gpihbp1*$^{-/-}$ mice, it bound avidly to the EC glycocalyx in BAT and heart capillaries but failed to mediate TRL margination. Thus, TRL margination along capillaries depends on the same Trp-rich loop that is required for triglyceride hydrolysis.

Confocal microscopy, electron microscopy, and NanoSIMS analyses were essential for the identification of glycocalyx LPL and for elucidating its relevance to TRL processing. Our first clue for the existence of "free LPL" within capillaries (i.e., LPL not attached to GPIHBP1) came from fluorescence microscopy experiments with the hLPL-specific mAb 88B8 (51), which does not detect GPIHBP1-bound LPL. When injected into *Lpl*$^{-/-}$ MCK–hLPL mice, 88B8 bound avidly to hLPL in heart capillaries, despite the inability to bind GPIHBP1-bound LPL. Super-resolution confocal microscopy, immunogold EM, and NanoSIMS analyses revealed that 88B8 bound to LPL in the glycocalyx—distant from 11A12 binding to GPIHBP1 on the luminal PM of ECs. The binding pattern for mAb 5D2, which binds to LPL's tryptophan-rich loop (50), was distinct. 5D2 bound to LPL in the same glycocalyx tufts as 88B8, but it also bound to GPIHBP1-bound LPL on the luminal PM, evident from strong colocalization between 5D2 and 11A12.

Glycocalyx-bound LPL was not a peculiarity of *Lpl*$^{-/-}$MCK–hLPL mice. We also observed glycocalyx LPL in *Lpl*$^{-/-}$Tie2–hLPL mice, where hLPL is produced by ECs. In those mice, 88B8 bound to hLPL in the glycocalyx, and 5D2 bound to both glycocalyx LPL and GPIHBP1-bound LPL. In *Gpihbp1*$^{-/-}$*Lpl*$^{-/-}$Tie2–hLPL mice, all of the LPL was located in the glycocalyx. Glycocalyx-bound LPL was not a peculiarity of hLPL. In capillaries of *Lpl*$^{+/-}$MCK–hLPL mice, hLPL and mLPL were detected in the same "glycocalyx tufts." In wild-type mice, mLPL in the glycocalyx was readily detected by immunogold electron microscopy (with gold-conjugated 27A7) and NanoSIMS analyses (with gold-conjugated Ab3174).

In earlier studies, we showed that GPIHBP1 moves bidirectionally across capillary ECs (abluminal to luminal, luminal to abluminal) (2, 34). We suspected that the capacity of GPIHBP1-bound and glycocalyx-bound LPL to move "backward" across ECs (from the luminal to the abluminal surface of ECs) could differ. Indeed, GPIHBP1-bound LPL (detected by 5D2) moves to the abluminal surface of ECs, whereas glycocalyx-bound LPL (detected by 88B8) remains within the capillary lumen. These findings imply that GPIHBP1 returns to the abluminal surface of capillaries before all of its LPL cargo is unloaded. The backward movement of LPL may seem inefficient, but we suspect that this inefficiency is the price to be paid for the existence of a mechanism for transporting LPL from the subendothelial spaces to the capillary lumen.

When recombinant hLPL was infused into *Gpihbp1*$^{-/-}$ mice, it bound avidly to the glycocalyx of capillaries, but it is noteworthy that the recombinant hLPL did not bind to larger blood vessels or to brain capillaries—implying that the properties of the glycocalyx in those vessels are distinct. Whether the robust binding of hLPL to the glycocalyx of heart and BAT capillaries is a consequence of larger amounts of sulfated glycosaminoglycans in those blood vessels is unknown.

In earlier studies with wild-type mice, we showed, with NanoSIMS analyses, that [^{2}H]TRLs marginate along capillaries, undergo lipolytic processing, and that the [^{2}H]TRL–derived lipids enter the mitochondria and cytosolic lipid droplets of cardiomyocytes within 2 min (52). In *Gpihbp1*$^{-/-}$ mice, where intravascular LPL is undetectable, the margination of [^{2}H]TRLs is virtually absent, and the uptake of [^{2}H]TRL-derived nutrients in cardiomyocytes is almost undetectable (52). In the current studies, we demonstrated, by electron microscopy, that glycocalyx LPL participates in TRL margination in wild-type mice. We also demonstrated that loading the glycocalyx of heart capillaries in *Gpihbp1*$^{-/-}$ mice with catalytically active hLPL results in robust TRL margination along capillaries. The next step was to test whether the loading of the glycocalyx with LPL in *Gpihbp1*$^{-/-}$ mice is accompanied by delivery of TRL-derived nutrients into cardiomyocytes. To explore this issue, we loaded the glycocalyx of heart capillary ECs in *Gpihbp1*$^{-/-}$ mice with catalytically active LPL, then infused [^{2}H]TRLs, and then measured (with NanoSIMS analyses) deuterium enrichment in the mitochondria and cytosolic lipid droplets of cardiomyocytes. In *Gpihbp1*$^{-/-}$ mice in which the glycocalyx had been loaded with LPL, we observed [^{2}H]TRL margination and, within 3 min, the entry of [^{2}H]TRL-derived nutrients into mitochondria and cytosolic fat droplets of cardiomyocytes. The fact that the fatty acids released by TRL processing in the EC glycocalyx would be taken up by cardiomyocytes (rather than being swept away in the bloodstream) is probably not surprising. The velocity of blood in capillaries is low [~0.5 mm/s (53)] and approaches zero (due to laminar flow) along the surface of ECs (54); this low velocity is important for the transit of many nutrients (not just TRL-derived nutrients) across capillary ECs. It is possible that the fatty acids released within the glycocalyx are bound by albumin and then escorted to the cardiomyocyte PM.

The lipolytic processing of TRLs is crucial for the delivery of lipid nutrients to parenchymal cells. To optimize lipid delivery, mammals evolved strategies to confine TRL processing to blood vessels that are immediately adjacent to parenchymal cells. One strategy is restricting GPIHBP1 expression (and LPL transport) to capillary ECs (2, 47). In heart and BAT, GPIHBP1 expression disappears as soon as the capillary diameter increases by ~50% (to become a very small venule) (2, 47). GPIHBP1 expression is also absent in brain capillaries (55). Our findings imply a second strategy for confining TRL processing to capillaries. Catalytically active LPL, when injected intravenously, binds to the glycocalyx lining of heart capillaries but not to the glycocalyx of larger blood vessels or brain capillaries. This finding could be physiologically relevant. If some of the LPL that is secreted by myocytes and adipocytes were to escape into the lymphatics and enter the systemic circulation, we suspect that it would be preferentially captured by the glycocalyx of capillaries of the heart and other peripheral tissues.

Materials and Methods

Genetically Modified Mice. *Gpihbp1*$^{-/-}$ mice (1), *Lpl*$^{-/-}$MCK–hLPL mice [*Lpl*$^{-/-}$ mice with a hLPL transgene driven by the promoter of the muscle creatine kinase gene (25)], and *Lpl*$^{-/-}$Tie2-hLPL mice [*Lpl*$^{-/-}$ mice with a hLPL transgene driven by the Tie2 promoter (30)] have been described previously.

Antibodies and Recombinant Proteins. mLPL was detected with rat monoclonal antibody (mAb) 27A7 and a rabbit polyclonal antibody (Ab3174) (47). Ab3174 binds to the N-terminal domain of mLPL, whereas 27A7 binds to LPL's C-terminal domain of mLPL (3). hLPL was detected with rabbit polyclonal antibody against hLPL (1256) (13), the LPL-specific mAb 5D2 [which binds to C-terminal Trp-rich loop distant from LPL's GPIHBP1-binding domains (26)], and mAb 88B8 [which binds to an epitope in LPL's GPIHBP1-binding domain (7)]. GPIHBP1 was detected with the rat mAb 11A12 (8). CD31 was detected with the hamster mAb 2H8 (Developmental Studies Hybridoma Bank, University of Iowa) (56). Recombinant hLPL and GPIHBP1 were prepared as described (3, 11). In addition, hLPL and a mutant hLPL with three tryptophan substitutions (W390A, W393A, and W394A) were produced as described (36). Methods to characterize the properties of antibodies 5D2, 88B8, 27A7, and Ab3174 are described in *SI Appendix, Supplemental Methods*.

Immunohistochemistry Studies. To detect human and mLPL in hearts from *Gpihbp1*$^{-/-}$*Lpl*$^{+/-}$MCK–hLPL mice, 10-μm-thick frozen sections were prepared, fixed with 3% paraformaldehyde (PFA), permeabilized with 0.2% Triton X-100 in PBS, and treated with M.O.M. Immunodetection Kit (Vector Laboratories, BMK-2202). Sections were incubated with mAbs against hLPL (88B8 or 5D2, 20 μg/mL) or the rabbit polyclonal antibody Ab3174 (8 μg/mL) at 4 °C overnight. Sections were washed three times to remove unbound antibodies and then incubated with Alexa Fluor 488–anti-mouse IgG or anti-rabbit IgG (Invitrogen, A-21202; Jackson ImmunoResearch, 711-545-152; 1:200 dilution). After washing, the sections were post-fixed with 3% PFA for 5 min, and cell nuclei were stained with DAPI. Images were obtained on an LSM980 microscope (Zeiss) with 20× or 63× objectives.

Assessing the Binding of Alexa Fluor–Labeled mAbs along the Luminal Surface of Capillaries. Mice were injected intravenously with Alexa Fluor 647–88B8, Alexa Fluor 555 5D2, and either Alexa Fluor 488–11A12 or Alexa Fluor 488–2H8 (150 to 500 μg each in 0.2 mL of PBS). After 2 min, mice were perfused with PBS (20 mL) through the left ventricle and then perfusion-fixed with 3% PFA (10 mL). The tissues were embedded in optimal cutting temperature (OCT) compound, and sections were processed for fluorescence microscopy. Images were recorded with an LSM980 microscope (Zeiss) with 20× or 63× objectives. Confocal micrographs of capillary cross-sections were captured with a Zeiss Airyscan detector and processed with Airyscan joint deconvolution (Zen Blue software v3.3).

For isolated mouse heart experiments, anesthetized *Gpihbp1*$^{+/+}$*Lpl*$^{-/-}$Tie2–hLPL and *Gpihbp1*$^{-/-}$*Lpl*$^{-/-}$Tie–hLPL mice were perfused with 10 mL of oxygenated Tyrode's solution (136 mM NaCl, 5.4 mM KCl, 0.33 mM NaH_2PO_4, 1 mM $MgCl_2$, 10 mM HEPES, pH 7.4, and 10 mM glucose) through the inferior vena cava. Hearts were removed, and the aorta was cannulated with a blunt-end 20-gauge needle and sutured in place. Hearts were flushed with Tyrode's solution, submerged in 30 mL of Tyrode's solution, and perfused with 1 mL of a solution containing Alexa Fluor 647–88B8, Alexa Fluor 555–5D2, and Alexa Fluor 488–11A12 (150 to 250 μg each). After 10 min, hearts were perfused with 3 mL Tyrode's solution followed by 3 mL of 3% PFA in PBS. The hearts were frozen in OCT and processed for fluorescence microscopy. Colocalization analyses were performed with Zen Blue software (Zeiss) or the EzColocalization plugin (57) in ImageJ.

In another study, anesthetized *Lpl*$^{-/-}$MCK–hLPL mice were perfused with 10 mL of Tyrode's solution through the inferior vena cava. Isolated hearts were flushed with Tyrode's solution, submerged in 30 mL of Tyrode's solution, and perfused with 2 mL of 3% PFA followed by 3 mL of Tyrode's solution containing 0.2% BSA and 5% donkey serum. Hearts were then perfused with 1 mL of a solution containing Alexa Fluor 647–11A12, Alexa Fluor 555–rat IgG, and Alexa Fluor 488–88B8 (150 to 250 μg each). After 10 min, hearts were perfused with 3 mL of Tyrode's solution, frozen in OCT, and processed for fluorescence microscopy.

Assessing Luminal to Abluminal Movement of LPL and GPIHBP1 across Capillary ECs. *Lpl*$^{-/-}$ MCK–hLPL mice were given an intravenous injection of Alexa Fluor–labeled 11A12, 88B8, and 5D2 (200 μg each). After 2 h, the mice were perfused with PBS (20 mL) through the left ventricle and then perfusion-fixed with 3% PFA (10 mL). BAT pads were embedded in OCT compound, and cryosections were prepared. Cross-sections of BAT capillaries containing an EC nucleus were imaged by fluorescent microscopy (2, 34). Relative levels of fluorescence on the luminal and abluminal surfaces of ECs were quantified with Zen Blue software (Zeiss).

In Vitro Studies to Investigate the Movement of hLPL from GPIHBP1-Coated Agarose Beads to Agarose Beads Coated with Heparin. Agarose beads were covalently coupled to mAb 11A12 according to the manufacturer's instructions (Thermo Fisher Scientific, 44894). After washing the beads with PBS/Ca/Mg and blocking for 1 h at 4 °C in StartingBlock buffer (Pierce, 37578), the beads were incubated for 30 min at 4 °C with purified recombinant mGPIHBP1 (1.2 μg) and purified recombinant hLPL (1 μg), or with hLPL alone. After washing the beads with PBS/Ca/Mg containing 0.2% NP40, heparin- or Protein A (ProA)–coated magnetic beads (CD Bioparticle, SMP-UM31; New England Biolabs, S1425S) were added and incubated for 30 min at 4 °C. Next, a magnet was used to retrieve the magnetic beads. After washing the 11A12-coated beads with PBS/Ca/Mg containing 0.2% NP40, GPIHBP1 and any GPIHBP1-bound LPL were released from the beads with 0.1 M glycine, pH 2.7 (followed by neutralization with 1 M Tris, pH 9.0). The heparin- or Protein A–magnetic beads were washed with 150 mM sodium chloride containing 20% glycerol, and any protein that remained attached to the beads was released by incubating in SDS-sample buffer at 70 °C for 10 min. The proteins were size-fractioned on a 4 to 12% SDS-polyacrylamide gel and transferred to nitrocellulose for immunoblotting. LPL was detected with IRDye800–Ab1256 (10 μg/mL), and GPIHBP1 was detected with IRDye680–11A12 (4 μg/mL). Antibody binding was visualized with an Odyssey infrared scanner (LI-COR).

Infusion of Recombinant hLPL into Mice. After cannulating isolated hearts from wild-type or *Gpihbp1*$^{-/-}$ mice, hearts were perfused with a 1 mL of Tyrode's solution containing 100 μg of recombinant hLPL or buffer alone. After 10 min, hearts were flushed with 3 mL Tyrode's solution and then perfused with a 1 mL solution containing Alexa Fluor 647–88B8, Alexa Fluor 555–27A7, and Alexa Fluor 555–11A12 or 2H8 (150 to 250 μg each). After 10 min, hearts were perfused with 3 mL of Tyrode's solution followed by 3 mL of 3% PFA in PBS, and then processed for fluorescence microscopy. In some cases, recombinant hLPL (100 μg) was injected intravenously into mice rather than into isolated, perfused hearts. In some experiments, a mutant hLPL (W390A, W393A, and W394A) (36) was infused into isolated hearts or injected intravenously.

Assessing TRL Margination in Blood Vessels by Confocal Microscopy. TRLs were isolated from the plasma of chow-fed *Gpihbp1*$^{-/-}$ mice by ultracentrifugation (35). *Gpihbp1*$^{-/-}$ or wild-type mice were injected intravenously through the inferior vena cava with recombinant hLPL (100 μg) and 5 μL of tetrahydrolipstatin (THL, 51 mM) or saline alone. TRL infusion experiments were carried out in two ways, depending on whether the goal was to detect TRL margination by fluorescence microscopy (Protocol 1) or electron microscopy (Protocol 2). Protocol 1: Three min after the infusion of hLPL, mice were perfused with Alexa Fluor 647–88B8 (250 μg), Alexa Fluor 555–2H8 (250 μg), and Alexa Fluor 488–TRLs (300 μg) along with 5 μL of 51 mM THL. After 3 min, the aorta was clamped, and hearts were perfused with 3 mL of PBS to remove unbound TRLs. Tissues were then processed for confocal microscopy as described earlier. Protocol 2: Three min after the infusion of hLPL, TRLs (300 μg) were injected intravenously through the inferior vena cava with 5 μL of 51 mM THL. After 3 min, the aorta was clamped and the hearts were perfused with 5 mL of HEPES/saline buffer (pH 7.2) containing 0.5% $LaCl_3$/$DyCl_3$, followed by perfusion-fixation with 10 mL of HEPES buffer (50 mM, pH7.2) containing 0.5% $LaCl_3$/$DyCl_3$ (Millipore Sigma, 203521-25G and 289272-25G) and 2.5% (vol/vol) glutaraldehyde (Electron Microscopy Sciences, 16222). Sections were prepared for transmission electron microscopy (52).

In related studies, *Gpihbp1*$^{-/-}$ mice were injected with [^{2}H]TRLs. To produce [^{2}H]TRLs, *Gpihbp1*$^{-/-}$ mice were placed on a fat-free (62% sucrose) diet (Envigo, TD.03314) for 13 d and then given uniformly labeled [^{2}H]mixed fatty acids (Cambridge Isotope Laboratories, DLM-8572-PK) by gastric gavage every 12 h for 4.5 d. [^{2}H]TRLs were collected as described (52). To monitor the hLPL-mediated [^{2}H]TRL processing, *Gpihbp1*$^{-/-}$ mice were injected with catalytically active recombinant hLPL (100 μg) through the inferior vena cava, thereby loading the capillary glycocalyx with LPL. Control *Gpihbp1*$^{-/-}$ mice were given saline alone. We suspected that the hLPL would be rapidly bound by the glycocalyx of capillaries (Fig. 7 and *SI Appendix*, Fig. S15) and therefore would rapidly disappear from the plasma compartment. To test that suspicion, plasma was obtained 3 min after the hLPL infusion and analyzed by immunoblotting. Plasma (0.4 μL) was size-fractioned on a 4 to 12% SDS-polyacrylamide gel, and the separated proteins were transferred to nitrocellulose. The transfer to nitrocellulose was confirmed with Ponceau S Red staining, and immunoblots were performed with IRDye680–88B8 (20 μg/mL). After 3 min, [^{2}H]TRLs (300 μg) were administered intravenously through the inferior vena cava. After 3 min, the hearts were clamped on the aortas and perfused with 5 mL of HEPES/saline buffer (pH 7.2) containing 0.5% $LaCl_3$/$DyCl_3$, followed by perfusion-fixation with 10 mL of HEPES buffer (50 mM, pH 7.2) containing 0.5% $LaCl_3$/$DyCl_3$ and 2.5% (vol/vol) glutaraldehyde. Tissue sections were then prepared for electron microscopy and NanoSIMS imaging (52).

Assessing TRL Margination in Blood Vessels by Electron Microscopy. Tissues were trimmed and sectioned to 65 nm with a Leica UC6 ultramicrotome. Sections were placed on 100-mesh copper grids that were coated sequentially

with formvar and carbon and then glow-discharged (Electron Microscopy Sciences, FCF 100-CU). The sections were stained with Reynold's lead citrate for 10 min and imaged at 200 kV with a Thermo T20 iCorr microscope equipped with a Gatan 4K camera or at 120 kV with Thermo T12 TEM equipped with a 2K camera.

For immunogold EM, mAbs 88B8, 5D2, and 11A12 were conjugated to 10-nm gold nanoparticles (Cytodiagnostics, CGN5K-10-3). The conjugates were subjected to two rounds of ultracentrifugation (40,000 × g, 45 min, 4 °C) to eliminate unbound gold nanoparticles. Then, 10-nm gold nanoparticle–conjugated 88B8 or 5D2 were injected into *Lpl*$^{-/-}$MCK–hLPL or wild-type mice through the vena cava or left ventricle. In the case of left ventricle injections, the heart was perfused with 0.5 mL of saline before the antibody infusion. Three min after antibodies were injected, hearts were perfused with 3 mL of normal saline containing 50 mM HEPES to remove unbound mAbs. Next, hearts were perfused with 5 mL HEPES/saline buffer (pH 7.2) containing 0.5% $LaCl_3$/$DyCl_3$ at a flow rate of 3 mL/min through the left ventricle. Finally, the hearts were perfusion-fixed through the left ventricle with 0.5% $LaCl_3$/$DyCl_3$ and 2.5% (vol/vol) glutaraldehyde in a 50 mM HEPES buffer (pH 7.2).

In another study, 10 mL of Tyrode's buffer containing 1 mM $CaCl_2$ was perfused into wild-type mice through the inferior vena cava. Hearts were then excised, cannulated, and perfused with 3 mL of Tyrode's buffer containing 1 mM $CaCl_2$ and 1% bovine serum albumin (BSA). The hearts were further perfused with 1 mL of Tyrode's buffer containing 1 mM $CaCl_2$, 1% BSA, and Ab3174 conjugated to 1.4 nm-gold nanoparticles (NanoProbes, 2025-30NMOL) and then submerged in Tyrode's buffer for 10 min at room temperature. After perfusion with 3 mL of Tyrode's buffer to remove unbound antibodies, hearts were perfused with 2 mL of HEPES/saline buffer (pH 7.2) containing 0.5% $LaNO_3$/$DyCl_3$, followed by perfusion-fixation with 0.5% $LaNO_3$/$DyCl_3$ (Millipore Sigma, 203548-25G) and 2.5% (vol/vol) glutaraldehyde in a 50 mM HEPES buffer (pH 7.2). In each study, the tip of the left ventricle, cut into 1 to 3 mm^3 pieces, was placed in 0.5% $LaCl_3$/$DyCl_3$ (or $LaNO_3$/$DyCl_3$) and 2.5% glutaraldehyde in a 50 mM HEPES buffer on ice for 1 h. Next, the samples were washed 5 times in 0.1 M sodium cacodylate buffer with 2.1% sucrose, pH 7.4 (5 min each, on ice). The tissues were then post-fixed in 2% OsO_4 (Electron Microscopy Sciences, 19190) and 0.1 M sodium cacodylate buffer (pH 7.4) on ice for 1 h. Samples were rinsed 5 times with distilled water (5 min each, on ice) and stained with 2% uranyl acetate (SPI-Chem, 6159-44-0) at 4 °C overnight. The tissues were then dehydrated and embedded in EMbed812 resin (Electron Microscopy Sciences, 14120) (52). BSE imaging and NanoSIMS analyses are described in *SI Appendix, Methods*.

Statistical Analyses. GraphPad Prism v9.0.2 was used for statistical analyses. Bar graphs show mean ± SEM. A two-tailed Student's *t* test was used for comparisons between two independent groups. For multiple group comparisons, one-way or two-way ANOVA tests were used.

Study Approval. Mice were fed a chow diet and were housed in a barrier facility with a 12-h light-dark cycle. All studies were approved by UCLA's Animal Research Committee according to guidelines described in the NIH Guide for the Care and Use of Laboratory Animals.

Data, Materials, and Software Availability. All study data are included in the article and/or *SI Appendix*.

ACKNOWLEDGMENTS. This work was supported by grants from the National Heart, Lung, and Blood Institute (HL087228, HL146358, HL139725), a Leducq Foundation Transatlantic Network Grant (19CVD04), an American Heart Association Postdoctoral Fellowship (23POST1011976), a Novo Nordisk Foundation Grant (NNF20OC0063444), and The John and Birthe Meyer Foundation, the Australian Research Council (LP190100433), and Research Grants Council of Hong Kong (17102722). We are grateful to Chris Allan and Patrick Heizer for working on the early phases of this project.

Author affiliations: [a]Department of Medicine, David Geffen School of Medicine, University of California, Los Angeles, CA 90095; [b]Department of Chemistry, The University of Hong Kong, Hong Kong, China; [c]School of Molecular Sciences, The University of Western Australia, Perth 6009, Australia; [d]Centre for Microscopy Characterisation and Analysis, The University of Western Australia, Perth 6009, Australia; [e]Division of Experimental Medicine, Beth Israel Deaconess Medical Center, Boston, MA 02215; [f]Department of Clinical Laboratory Medicine, Gunma University School of Medicine, Maebashi 371-8511, Japan; [g]Department of Pathology and Laboratory Medicine, University of California, Los Angeles, CA 90095; [h]Finsen Laboratory, Copenhagen University Hospital-Rigshospitalet, Copenhagen N DK–2200, Denmark; [i]Biotech Research and Innovation Centre, University of Copenhagen, Copenhagen N DK-2200, Denmark; and [j]Department of Human Genetics, David Geffen School of Medicine, University of California, Los Angeles, CA 90095

1. A. P. Beigneux *et al.*, Glycosylphosphatidylinositol-anchored high density lipoprotein–binding protein 1 plays a critical role in the lipolytic processing of chylomicrons. *Cell Metab.* **5**, 279–291 (2007).
2. B. S. J. Davies *et al.*, GPIHBP1 is responsible for the entry of lipoprotein lipase into capillaries. *Cell Metab.* **12**, 42–52 (2010).
3. G. Birrane *et al.*, Structure of the lipoprotein lipase–GPIHBP1 complex that mediates plasma triglyceride hydrolysis. *Proc. Natl. Acad. Sci. U.S.A.* **116**, 1723–1732 (2019).
4. S. Mysling *et al.*, The acidic domain of the endothelial membrane protein GPIHBP1 stabilizes lipoprotein lipase activity by preventing unfolding of its catalytic domain. *Elife* **5**, e12095 (2016).
5. S. Mysling *et al.*, The angiopoietin-like protein ANGPTL4 catalyzes unfolding of the hydrolase domain in lipoprotein lipase and the endothelial membrane protein GPIHBP1 counteracts this unfolding. *Elife* **5**, e20958 (2016).
6. K. Z. Leth-Espensen *et al.*, The intrinsic instability of the hydrolase domain of lipoprotein lipase facilitates its inactivation by ANGPTL4-catalyzed unfolding. *Proc. Natl. Acad. Sci. U.S.A.* **118**, e2026650118 (2021).
7. C. M. Allan *et al.*, An LPL–specific monoclonal antibody, 88B8, that abolishes the binding of LPL to GPIHBP1. *J. Lipid Res.* **57**, 1889–1898 (2016).
8. A. P. Beigneux *et al.*, Highly conserved cysteines within the Ly6 domain of GPIHBP1 are crucial for the binding of lipoprotein lipase. *J. Biol. Chem.* **284**, 30240–30247 (2009).
9. A. P. Beigneux *et al.*, GPIHBP1 missense mutations often cause multimerization of GPIHBP1 and thereby prevent lipoprotein lipase binding. *Circ. Res.* **116**, 624–632 (2015).
10. A. P. Beigneux *et al.*, Assessing the role of the glycosylphosphatidylinositol-anchored high density lipoprotein–binding protein 1 (GPIHBP1) three-finger domain in binding lipoprotein lipase. *J. Biol. Chem.* **286**, 19735–19743 (2011).
11. K. K. Kristensen *et al.*, A disordered acidic domain in GPIHBP1 harboring a sulfated tyrosine regulates lipoprotein lipase. *Proc. Natl. Acad. Sci. U.S.A.* **115**, E6020–E6029 (2018).
12. W. Song *et al.*, Electrostatic sheathing of lipoprotein lipase is essential for its movement across capillary endothelial cells. *J. Clin. Invest.* **132**, e157500 (2022).
13. A. P. Beigneux *et al.*, Lipoprotein lipase is active as a monomer. *Proc. Natl. Acad. Sci. U.S.A.* **116**, 6319–6328 (2019).
14. A. Kumari *et al.*, Inverse effects of APOC2 and ANGPTL4 on the conformational dynamics of lid-anchoring structures in lipoprotein lipase. *Proc. Natl. Acad. Sci. U.S.A.* **120**, e2221888120 (2023).
15. E. D. Korn, Clearing factor, a heparin-activated lipoprotein lipase. I. Isolation and characterization of the enzyme from normal rat heart. *J. Biol. Chem.* **215**, 1–14 (1955).
16. S. Reitsma, D. W. Slaaf, H. Vink, M. A. M. J. Van Zandvoort, M. G. A. oude Egbrink, The endothelial glycocalyx: Composition, functions, and visualization. *Pflügers Arch.* **454**, 345–359 (2007).
17. A. L. Jones, J. M. Price, Some methods of electron microscopic visualization of lipoproteins in plasma and chyle. *J. Histochem. Cytochem.* **16**, 366–370 (1968).
18. L. Jonasson, G. K. Hansson, G. Bondjers, G. Bengtsson, T. Olivecrona, Immunohistochemical localization of lipoprotein lipase in human adipose tissue. *Atherosclerosis* **51**, 313–326 (1984).
19. M. O. Pentikäinen, R. Oksjoki, K. Öörni, P. T. Kovanen, Lipoprotein lipase in the arterial wall: Linking LDL to the arterial extracellular matrix and much more. *Arterioscler. Thromb. Vasc. Biol.* **22**, 211–217 (2002).
20. L. Camps, M. Reina, M. Llobera, S. Vilaro, T. Olivecrona, Lipoprotein lipase: Cellular origin and functional distribution. *Am. J. Physiol.* **258**, C673–C681 (1990).
21. D. Bessesen, C. Richards, J. Etienne, J. Goers, R. Eckel, Spinal cord of the rat contains more lipoprotein lipase than other brain regions. *J. Lipid Res.* **34**, 229–238 (1993).
22. E. J. Blanchette-Mackie, H. Masuno, N. K. Dwyer, T. Olivecrona, R. O. Scow, Lipoprotein lipase in myocytes and capillary endothelium of heart: Immunocytochemical study. *Am. J. Physiol.* **256**, E818–E828 (1989).
23. A. Casanovas, M. Carrascal, J. Abian, M. D. Lopez-Tejero, M. Llobera, Application of proteomic tools to detect the nonspecificity of a polyclonal antibody against lipoprotein lipase. *J. Proteome Res.* **7**, 4173–4177 (2008).
24. G. Mertens, J. J. Cassiman, H. Van den Berghe, J. Vermylen, G. David, Cell surface heparan sulfate proteoglycans from human vascular endothelial cells. Core protein characterization and antithrombin III binding properties. *J. Biol. Chem.* **267**, 20435–20443 (1992).
25. S. Levak-Frank *et al.*, Induced mutant mice expressing lipoprotein lipase exclusively in muscle have subnormal triglycerides yet reduced high density lipoprotein cholesterol levels in plasma. *J. Biol. Chem.* **272**, 17182–17190 (1997).
26. J. G. Luz *et al.*, The structural basis for monoclonal antibody 5D2 binding to the tryptophan-rich loop of lipoprotein lipase. *J. Lipid Res.* **61**, 1347–1359 (2020).
27. P. H. Weinstock *et al.*, Severe hypertriglyceridemia, reduced high density lipoprotein, and neonatal death in lipoprotein lipase knockout mice. Mild hypertriglyceridemia with impaired low density lipoprotein clearance in heterozygotes. *J. Clin. Invest.* **96**, 2555–2568 (1995).
28. K. W. Dunn, M. M. Kamocka, J. H. McDonald, A practical guide to evaluating colocalization in biological microscopy. *Am. J. Physiol. Cell Physiol.* **300**, 723–742 (2011).
29. V. Zinchuk, O. Grossenbacher-Zinchuk, Quantitative colocalization analysis of confocal fluorescence microscopy images. *Curr. Protoc. Cell Biol.* **52**, 4–19 (2008).
30. M. Takahashi *et al.*, In vivo arterial lipoprotein lipase expression augments inflammatory responses and impairs vascular dilatation. *Arterioscler. Thromb. Vasc. Biol.* **28**, 455–462 (2008).
31. B. S. Davies *et al.*, An accumulation of non-farnesylated prelamin A causes cardiomyopathy but not progeria. *Hum. Mol. Genet.* **19**, 2682–2694 (2010).

32. B. Holzer *et al.*, Characterization of covalently bound anti-human immunoglobulins on self-assembled monolayer modified gold electrodes. *Adv. Biosyst.* **1**, 1700055 (2017).
33. H. Jiang *et al.*, High–resolution imaging of dietary lipids in cells and tissues by NanoSIMS analysis. *J. Lipid Res.* **55**, 2156–2166 (2014).
34. B. S. Davies *et al.*, Assessing mechanisms of GPIHBP1 and lipoprotein lipase movement across endothelial cells. *J. Lipid Res.* **53**, 2690–2697 (2012).
35. C. N. Goulbourne *et al.*, The GPIHBP1–LPL complex is responsible for the margination of triglyceride-rich lipoproteins in capillaries. *Cell Metab.* **19**, 849–860 (2014).
36. A. M. Lund Winther, K. K. Kristensen, A. Kumari, M. Ploug, Expression and one-step purification of active lipoprotein lipase contemplated by biophysical considerations. *J. Lipid Res.* **62**, 100149 (2021).
37. E. D. Korn, Clearing factor, a heparin-activated lipoprotein lipase. II. Substrate specificity and activation of coconut oil. *J. Biol. Chem.* **215**, 15–26 (1955).
38. A. J. Hoogewerf, L. A. Cisar, D. C. Evans, A. Bensadoun, Effect of chlorate on the sulfation of lipoprotein lipase and heparan sulfate proteoglycans. Sulfation of heparan sulfate proteoglycans affects lipoprotein lipase degradation. *J. Biol. Chem.* **266**, 16564–16571 (1991).
39. L. A. Cisar, A. J. Hoogewerf, M. Cupp, C. A. Rapport, A. Bensadoun, Secretion and degradation of lipoprotein lipase in cultured adipocytes. Binding of lipoprotein lipase to membrane heparan sulfate proteoglycans is necessary for degradation. *J. Biol. Chem.* **264**, 1767–1774 (1989).
40. K. Shimada, P. J. Gill, J. E. Silbert, W. H. Douglas, B. L. Fanburg, Involvement of cell surface heparin sulfate in the binding of lipoprotein lipase to cultured bovine endothelial cells. *J. Clin. Invest.* **68**, 995–1002 (1981).
41. P. Gin *et al.*, Binding preferences for GPIHBP1, a glycosylphosphatidylinositol-anchored protein of capillary endothelial cells. *Arterioscler. Thromb. Vasc. Biol.* **31**, 176–182 (2011).
42. P. Gin *et al.*, The acidic domain of GPIHBP1 is important for the binding of lipoprotein lipase and chylomicrons. *J. Biol. Chem.* **284**, 29554–29562 (2008).
43. W. Plengpanich *et al.*, Multimerization of glycosylphosphatidylinositol-anchored high density lipoprotein–binding protein 1 (GPIHBP1) and familial chylomicronemia from a serine-to-cysteine substitution in GPIHBP1 Ly6 domain. *J. Biol. Chem.* **289**, 19491–19499 (2014).
44. C. V. Voss *et al.*, Mutations in lipoprotein lipase that block binding to the endothelial cell transporter GPIHBP1. *Proc. Natl. Acad. Sci. U.S.A.* **108**, 7980–7984 (2011).
45. A. P. Beigneux *et al.*, Chylomicronemia with a mutant GPIHBP1 (Q115P) that cannot bind lipoprotein lipase. *Arterioscler. Thromb. Vasc. Biol.* **29**, 956–962 (2009).
46. C. M. Allan *et al.*, Mutating a conserved cysteine in GPIHBP1 reduces amounts of GPIHBP1 in capillaries and abolishes LPL binding. *J. Lipid Res.* **58**, 1453–1461 (2017).
47. W. Song *et al.*, Intracapillary LPL levels in brown adipose tissue, visualized with an antibody-based approach, are regulated by ANGPTL4 at thermoneutral temperatures. *Proc. Natl. Acad. Sci. U.S.A.* **120**, e2219833120 (2023).
48. R. O. Scow, T. Olivecrona, Effect of albumin on products formed from chylomicron triacylclycerol by lipoprotein lipase in vitro. *Biochim. Biophys. Acta* **487**, 472–486 (1977).
49. A. Lookene, N. B. Groot, J. J. Kastelein, G. Olivecrona, T. Bruin, Mutation of tryptophan residues in lipoprotein lipase. Effects on stability, immunoreactivity, and catalytic properties. *J. Biol. Chem.* **272**, 766–772 (1997).
50. J. Luz *et al.*, The structural basis for monoclonal antibody 5D2 binding to the tryptophan–rich loop of lipoprotein lipase. *J. Lipid Res.* **61**, 1347–1359 (2020).
51. C. M. Allan *et al.*, An LPL-specific monoclonal antibody, 88B8, that abolishes the binding of LPL to GPIHBP1. *J. Lipid Res.* **57**, 1889–1898 (2016).
52. C. He *et al.*, NanoSIMS analysis of intravascular lipolysis and lipid movement across capillaries and into cardiomyocytes. *Cell Metab.* **27**, 1055–1066 (2018).
53. K. P. Ivanov, M. K. Kalinina, Y. I. Levkovich, Blood flow velocity in capillaries of brain and muscles and its physiological significance. *Microvasc. Res.* **22**, 143–155 (1981).
54. T. E. Kornfield, E. A. Newman, Measurement of retinal blood flow using fluorescently labeled red blood cells. *eNeuro* **2**, ENEURO.0005-15.2015 (2015).
55. M. Vanlandewijck *et al.*, A molecular atlas of cell types and zonation in the brain vasculature. *Nature* **554**, 475–480 (2018).
56. S. A. Bogen, H. S. Baldwin, S. C. Watkins, S. M. Albelda, A. K. Abbas, Association of murine CD31 with transmigrating lymphocytes following antigenic stimulation. *Am. J. Pathol.* **141**, 843–854 (1992).
57. W. Stauffer, H. Sheng, H. N. Lim, EzColocalization: An ImageJ plugin for visualizing and measuring colocalization in cells and organisms. *Sci. Rep.* **8**, 15764 (2018).